Article ID: 1007-4627(2017) 02-0242-10

Relativistic Compton Profile of H-like Ions

WAN Jianjie

(*College of Physics and Electronic Engineering, Northwest Normal University, Lanzhou 730070, China*)

Abstract: The Compton profiles of the electron in the ground and excited states of H-like ions have been calculated systematically with one-electron Dirac radial orbitals by using the proper Fourier transformation. Taking the H atom and Xe^{53+} ion as examples, the effects of relativity and finite nuclear size on Compton profile have been discussed. Furthermore, the dependence of one-electron Compton profile on the principle quantum number n, orbital quantum number l, angular quantum number j and nuclear charge Z has also been discussed. It is found that the relativistic effect can expand the distribution of the Compton profile and split the orbital more and more obviously for given $nl(l \neq 0)$ as increasing Z. However, the relativistic effect can gradually weaken with the increase of the principal quantum number n and orbital quantum number l. Furthermore, the Compton profile of the orbital with quantum number nl_j has certain number of platforms that is $n-l$. In addition, the nuclear finite size hardly affects the Compton profile for H atom and Xe^{53+} ion.

Key words: Compton profile; relativistic effect; electron momentum distribution; H-like ion

CLC number: O571.6; P142.9 **Document code:** A **DOI:** 10.11804/NuclPhysRev.34.02.242

1 Introduction

Compton scattering is an effective and special way to obtain the information on the electron momentum distribution (EMD) in atoms/ions, molecules and surface[1–5]. From the theoretical point of view, the differential cross section is proportional to the Compton profile in the so-called impulse approximation

$$J(p_z) = \iint \rho(p_x, p_y, p_z) \mathrm{d}p_x \mathrm{d}p_y \ , \qquad (1)$$

where $\rho(p_x, p_y, p_z)$ is the electron probability density in momentum space in target before scattering, p_z is the component of the electron momentum along the scattering vector. It is stated that the distribution of electron momentum can be used to reveal many interesting features which are not obviously shown in spatial distribution of electron even though they are in accordance with each other in many literatures. The Compton profile $J(p_z)$ is directly related to the momentum density $\rho(p_x, p_y, p_z)$, on the other hand, so the Compton profile can supply a way to check the accuracy of wavefuntion. Furthermore, $J(p_z)$ can be measured in experiment and the Compton profile of atom or molecule determines the envelope of the differential cross sections, for example, in radiative electron capture (REC) and resonant transfer and excitation (RTE) processes in ion-atom/molecule collision besides the Compton scattering. In REC and RTE, the projectile ions can capture the electron in the bound state of target atoms/molecules, and then the combined system radiates a photon or photons. Therefore, the information of electron energy and momentum in target atoms/molecules can be revealed through the envelope of the radiative spectra.

In the last decades, there are much typical theoretical work. Currat *et al.*[6] carried out the calculations of the core contributions to the Compton profiles for Li, C and Al by using excited-state one-electron continuum wavefunctions evaluated in the ground-state Hartree-Fock-Slater potential of the nucleus and remaining electrons. Their results were in good agreement with the impulse approximation. Pant *et al.*[7] calculated the Compton profiles for atomic Ne, Ar, and Kr by using a variationally optimized effective-potential model. The Compton profiles of Ne, Ar, and Kr were also calculated from ground-state energies and wavefunction using the Kohn-Sham self-consistent scheme in the local-density approximation (LDA) by Tong *et al.*[8]. They found their results are closer to the experimental values from Hartree-Fock results and

Received date: 8 June 2016; **Revised date:** 18 Sep. 2016

Foundation item: National Natural Science Foundation of China(11204243); Natural Science Foundation of Gansu Province, China(1506RJYA131); Scientific Research Foundation of Physics of CPEE-NWNU

Biography: WAN Jianjie (1982–), male, Tianshui, Gansu, Associate professor, working on atomic physics;
E-mail: wanjj@nwnu.edu.cn.

there are some numerical problems in the calculation for large atoms. Mukhopadhyaya *et al.*[9] obtained the atomic Compton profiles of Ne, Na, Mg, Al, Si and Ar in the form factor or exact hydrogenic approximation with nonrelativistic Coulomb functions in the spherical polar coordinates. In the work by Parr *et al.*[10], the phase-space distribution function corresponding to a gound-state density of a many-electron system is explored as a means for generation of momentum-space properties through density-functional theory. Holm[11] discussed a rigorous relativistic treatment of the differential cross section for Compton scattering from bound electron states and found a simple expression with the help of relativistic central-field Hartree-Fock wavefunctions. Karim[12, 13] calculated the orbtial and total Compton profile of the ground states of O and Ne and their ions in different stages with Hartree-Fock (HF) wavefunctions. Li *et al.*[14] used discrete variation method to study the momentum profiles of atomic He, Ar, Na and K based on density functional theory (DFT). Harbola *et al.*[15] studied the Compton profiles of closed-shell atomic He, Be and Ne in their ground state and the singlet excited state for He, with employing DFT. Jaiswal and Shukla[16] computed the total Compton profiles of He, Ne, Ar, Kr, Xe and Rn in ground states, using the Dirac-Hartree-Fock formalism with kinetically balanced Gaussian basis functions. Mou *et al.*[17] calculated the single-electron momentum density distribution and the total Compton profiles for He ($1s^2$), Ne ($1s^22s^22p^6$), Ar ($1s^22s^22p^63s^23p^6$), Kr ($1s^22s^22p^63s^23p^63d^{10}4s^24p^6$) and Xe ($1s^22s^22p^63s^23p^63d^{10}4s^24p^64d^{10}5s^25p^6$). In their work, the single-electron radial wavefunctions in coordinate space are obtained from Hartree-Fock with relativistic corrections (HFR) method.

Besides, there have also been some systematical good calculations. For example, Biggs *et al.*[18] used the HF and relativistic Dirac-Hartree-Fock (DHF) wavefunctions to calculate the orbital and total Compton profile in the ground states of atoms with $Z = 1 \sim 36$ and $Z = 36 \sim 102$, respectively. Thakkar *et al.*[19] calculated the first three coefficients in each of the small p Maclaurin and large p asymptotic expansions of the spherically averaged electron momentum densities of the ground states of the 103 neutral atoms from H through Lr, 73 cations from Li^+ to Ra^+ and 41 anions from Li^- to I^-, with employing the nonrelativistic self-consistent-field (SCF) wavefunctions. The coefficients can be used to analyze the experimental Compton profiles. Koga *et al.*[20, 21] calculated the Compton profile of He and constructed the numerical Hartree-Fock momentum densities for the neutral atoms from H to Lr ($Z = 1 \sim 103$).

As is known, the available Compton profiles were almost calculated from the electron radial orbital generated in central field approximation and were aimed at near-neutral ions and atoms. In fact, one-electron radial orbitals can also consider the electron correlation through multiconfiguration self-consistent-field methods indeed. However, only the single-electron properties have been focused on in the present calculation because of the lack of a systematic analysis on one-electron Compton profile in past years. As such, the one-electron Compton profiles in the ground and excited states have been calculated systematically for H-like ions, taking examples of H atom and Xe^{53+} ion because of their frequent use in experiments, and the relativistic effects, as well as the nucleus volume effects, on them have also been discussed, where the nucleus volume effects can be extracted by comparing the present results with the analytic relativistic Compton profile. In Sec. 2, we provide a detailed description of the theoretical method and computational procedure. In Sec. 3, firstly, the Compton profiles are shown for H atom and Xe^{53+} ion. Then, extensive comparison with other theoretical results were given in detail, while the dependence on the principle quantum number n and relativistic orbital quantum number κ or l_j and those effects from relativity and the nucleus volume mentioned above have also been found and analyzed in detail. Finally, some concluding remarks and outlook are summarized in Sec. 4.

2 Theoretical method

In the relativistic central field, a particular nl orbital breaks up into two orbitals, one with $j = l - \frac{1}{2}$ and the other one with $j = l + \frac{1}{2}$ except for s orbital, to which only the latter can exist. Therefore, a subscript j or κ is usually added in order to specify the orbital completely. The relativistic one-electron wavefunctions are usually written as in the form[22–24]

$$\psi_{n\kappa m}(r,\theta,\phi) = \frac{1}{r}\begin{pmatrix} P_{n\kappa}(r)\chi_{\kappa m}(\theta,\phi) \\ iQ_{n\kappa}(r)\chi_{-\kappa m}(\theta,\phi) \end{pmatrix}. \quad (2)$$

For either of the $n\kappa$ orbitals, the radial wavefunction is described by two components: $P_{n\kappa}(r)$, a large component that looks very much like the nonrelativistic wavefunction for the atoms and ions with low Z, and $Q_{n\kappa}(r)$, the small component. Both of them can be obtained by solving Dirac equations with Fermi two-parameter model describing the distribution of nuclear charge[22, 23]. κ is the (relativistic) angular momentum quantum number, *i.e.* $\kappa = \pm(j + \frac{1}{2})$ for $j = l \mp \frac{1}{2}$ and the functions $\chi_{\kappa m}(\theta,\phi)$ are spinor spherical harmonics[22]. For this form, the normalization

condition is

$$\int_0^\infty [(P_{n\kappa}(r))^2+(Q_{n\kappa}(r))^2]\mathrm{d}r=1\ . \tag{3}$$

In the impulse approximation[1, 3, 9, 16], the calculation of Compton profiles can be carried out by using the following expression in atomic units, *i.e.*

$$J_{n\kappa}(q)=\frac{1}{2}\int_q^\infty \frac{I_{n\kappa}(p)}{p}\mathrm{d}p\ . \tag{4}$$

where q is a certain value with expressed in atomic units of $\frac{me^2}{\hbar}$, and the single-electron Compton profile must satisfy the condition

$$2\int_0^\infty J_{n\kappa}(q)\mathrm{d}q=1\ . \tag{5}$$

In the present calculation, the maximum momentum of 200 a.u. was chosen as the upper limit for numerical integration; the larger it was, the more accurate Compton profile we obtained. From the physical picture, the most general form for q is given as the projection of the initial electron momentum $\boldsymbol{p}$ on the momentum transfer $\boldsymbol{k}$. That is

$$q=-\frac{\boldsymbol{k}\cdot\boldsymbol{p}}{k}. \tag{6}$$

$I_{n\kappa}(p)$ is the electron momentum density for electrons of momentum p, which is given as

$$I_{n\kappa}(p)=[(\gamma^P_{n\kappa}(p))^2+(\gamma^Q_{n\kappa}(p))^2]p^2\ , \tag{7}$$

where $\gamma^P_{n\kappa}(p)$ and $\gamma^Q_{n\kappa}(p)$ are defined as the Fourier transform of the spatial wavefunction $P_{n\kappa}(r)$ and $Q_{n\kappa}(r)$, and then are given by respectively[11, 18]

$$\gamma^P_{n\kappa}(p)=\sqrt{\frac{2}{\pi}}\int_0^\infty P_{n\kappa}(r)j_l(pr)r\mathrm{d}r\ , \tag{8}$$

and

$$\gamma^Q_{n\kappa}(p)=\begin{cases}\sqrt{\frac{2}{\pi}}\int_0^\infty Q_{n\kappa}(r)j_{l+1}(pr)r\mathrm{d}r, & j=l+\frac{1}{2}\\ \sqrt{\frac{2}{\pi}}\int_0^\infty Q_{n\kappa}(r)j_{l-1}(pr)r\mathrm{d}r, & j=l-\frac{1}{2}\end{cases} \tag{9}$$

where $j_l(pr)$ is a spherical Bessel function of the first kind. Note that in the nonrelativistic limit $\gamma^P_{n\kappa}(p)$ becomes the momentum transform of the radial nonrelativistic spatial wavefunctions and $\gamma^Q_{n\kappa}(p)$ goes to zero. In other words, the relativistic Compton profile Eq. (4) also goes over to the correct limit[18].

3 Results and discussion

3.1 Compton profile of the ground state $1s$ in H atom and Xe^{53+} ion

Table 1 lists the values of Compton profiles for the ground state $1s$ of H atom and Xe^{53+} ion. In Table 1, the present results have been given by three methods labelled as a, b and c, respectively. The calculation a is that the Compton profile was calculated from the relativistic radial orbitals obtained by solving Dirac equations numerically with two-parameter Fermi nuclear model. The calculation b shows the Compton profile calculated with analytical relativistic radial wavefunction Eqs. (12) and (13) as below. The calculation c gives the Compton profile calculated with analytical nonrelativistic Compton profiles Eq. (11) from Eq. (10) as below. From the table, the present Compton profiles of $1s$ of H atom are in good agreement with the available nonrelativistic results[18].

As is well known, the nonrelativistic single-electron orbital in point Coulomb potential can be given by[25]

$$P_{nl}(r)=N_{nl}r^{l+1}\mathrm{e}^{-\frac{Z}{n}r}F(-(n-l-1),2l+2;\frac{2Z}{n}r)\ , \tag{10}$$

Table 1 Compton profile for the ground state $1s$ of H atom and Xe^{53+} ion.

q	H atom				Xe^{53+} ion		
	This work[a]	This work[b]	This work[c]	Ref. [18]	This work[a]	This work[b]	This work[c]
0.00	8.487 7(−1)	8.487 7(−1)	8.488 3(−1)	8.49(−1)	1.467 2(−2)	1.468 4(−2)	1.571 9(−2)
0.05	8.424 3(−1)	8.424 3(−1)	8.424 9(−1)	8.42(−1)	1.467 2(−2)	1.468 4(−2)	1.571 9(−2)
0.10	8.238 1(−1)	8.238 1(−1)	8.238 6(−1)	8.24(−1)	1.467 2(−2)	1.468 4(−2)	1.571 9(−2)
0.15	7.939 7(−1)	7.939 7(−1)	7.940 2(−1)	7.94(−1)	1.467 1(−2)	1.468 4(−2)	1.571 9(−2)
0.20	7.545 7(−1)	7.545 6(−1)	7.546 0(−1)	7.55(−1)	1.467 1(−2)	1.468 4(−2)	1.571 8(−2)
0.30	6.554 3(−1)	6.554 3(−1)	6.554 5(−1)	6.55(−1)	1.467 1(−2)	1.468 3(−2)	1.571 8(−2)
0.40	5.438 1(−1)	5.438 0(−1)	5.438 1(−1)	5.44(−1)	1.467 0(−2)	1.468 2(−2)	1.571 6(−2)
0.50	4.346 1(−1)	4.346 1(−1)	4.346 0(−1)	4.35(−1)	1.466 8(−2)	1.468 1(−2)	1.571 5(−2)
0.60	3.374 6(−1)	3.374 6(−1)	3.374 4(−1)	3.37(−1)	1.466 7(−2)	1.467 9(−2)	1.571 3(−2)
0.70	2.566 2(−1)	2.566 2(−1)	2.566 0(−1)	2.57(−1)	1.466 5(−2)	1.467 8(−2)	1.571 1(−2)

Table 1 (Continued)

q	H atom				Xe^{53+} ion		
	This work[a]	This work[b]	This work[c]	Ref. [18]	This work[a]	This work[b]	This work[c]
0.80	1.924 5(−1)	1.924 5(−1)	1.924 4(−1)	1.92(−1)	1.466 3(−2)	1.467 6(−2)	1.570 9(−2)
1.00	1.061 2(−1)	1.061 2(−1)	1.061 0(−1)	1.06(−1)	1.4658(−2)	1.4671(−2)	1.570 3(−2)
1.20	5.844 0(−2)	5.844 0(−2)	5.843 2(−2)	5.84(−2)	1.4652(−2)	1.466 5(−2)	1.569 6(−2)
1.40	3.273 5(−2)	3.273 5(−2)	3.273 0(−2)	3.27(−2)	1.464 5(−2)	1.465 7(−2)	1.568 7(−2)
1.60	1.881 7(−2)	1.881 7(−2)	1.881 3(−2)	1.88(−2)	1.463 6(−2)	1.464 9(−2)	1.567 8(−2)
1.80	1.113 8(−2)	1.113 8(−2)	1.113 6(−2)	1.11(−2)	1.462 7(−2)	1.464 0(−2)	1.566 7(−2)
2.00	6.792 2(−3)	6.792 2(−3)	6.790 6(−3)	6.79(−3)	1.461 7(−2)	1.462 9(−2)	1.565 4(−2)
2.40	2.748 6(−3)	2.748 5(−3)	2.747 8(−3)	2.75(−3)	1.459 2(−2)	1.460 5(−2)	1.562 6(−2)
3.00	8.491 5(−4)	8.491 5(−4)	8.488 3(−4)	8.49(−4)	1.454 8(−2)	1.456 1(−2)	1.557 4(−2)
4.00	1.728 7(−4)	1.728 7(−4)	1.727 7(−4)	1.73(−4)	1.445 3(−2)	1.446 5(−2)	1.546 3(−2)
5.00	4.833 5(−5)	4.833 4(−5)	4.829 5(−5)	4.83(−5)	1.433 1(−2)	1.434 4(−2)	1.532 2(−2)
6.00	1.677 6(−5)	1.677 6(−5)	1.675 8(−5)	1.68(−5)	1.418 5(−2)	1.419 8(−2)	1.515 1(−2)
7.00	6.800 5(−6)	6.800 1(−6)	6.790 6(−6)	6.79(−6)	1.401 5(−2)	1.402 8(−2)	1.495 2(−2)
8.00	3.095 0(−6)	3.096 3(−6)	3.090 9(−6)	3.09(−6)	1.382 2(−2)	1.383 5(−2)	1.472 8(−2)
10.00	8.260 9(−7)	8.259 9(−7)	8.238 6(−7)	8.20(−7)	1.337 3(−2)	1.338 6(−2)	1.420 7(−2)
15.00	7.398 3(−8)	7.392 9(−8)	7.353 5(−8)	7.40(−8)	1.196 2(−2)	1.197 5(−2)	1.257 7(−2)
20.00	1.328 6(−8)	1.328 4(−8)	1.316 4(−8)	1.30(−8)	1.030 8(−2)	1.032 2(−2)	1.068 9(−2)
30.00	1.185 3(−9)	1.183 3(−9)	1.160 5(−9)	1.20(−9)	7.019 2(−3)	7.033 1(−3)	7.013 9(−3)
40.00	2.170 2(−10)	2.139 0(−10)	2.068 4(−10)	2.30(−10)	4.435 4(−3)	4.449 5(−3)	4.231 8(−3)
60.00	1.979 9(−11)	1.954 3(−11)	1.817 8(−11)	4.30(−11)	1.644 4(−3)	1.658 5(−3)	1.408 8(−3)
100.00	1.008 0(−12)	1.022 2(−12)	8.485 7(−13)	2.60(−11)	2.608 8(−4)	2.748 5(−4)	1.808 9(−4)

a Relativistic radial orbitals obtained by solving Dirac equations numerically with two-parameter Fermi nuclear model.
b Calculated with analytical relativistic radial wavefunction Eqs. (12) and (13).
c Calculated with analytical nonrelativistic Compton profile Eq. (11) from Eq. (10).

where $N_{nl} = \frac{(\frac{2Z}{n})^{l+\frac{3}{2}}}{(2l+1)!}\sqrt{\frac{(n+l)!}{(n-l-1)!2n}}$ and F is confluent hypergeometric function. Then, according to the appropriate Fourier transformation[11, 18], the single-electron Compton profile is also expressed analytically as follows, taking the nonrelativistic Compton profile of $1s$ orbital of H-like ion as an example,

$$J_{1s}(q) = \frac{8Z^5}{3\pi}\frac{1}{(q^2+Z^2)^3}. \tag{11}$$

On the other hand, it is well known that the relativistic radial function for H-like system in point Coulomb field can be written as[26]

$$P_{n\kappa}(r) = \sqrt{2-\frac{\epsilon}{c^2}}\xi(\frac{\rho}{N})^{\gamma}\mathrm{e}^{-\frac{\rho}{2N}}[-n_rF_1+(N-\kappa)F_2], \tag{12}$$

$$Q_{n\kappa}(r) = -\sqrt{\frac{\epsilon}{c^2}}\xi(\frac{\rho}{N})^{\gamma}\mathrm{e}^{-\frac{\rho}{2N}}[n_rF_1+(N-\kappa)F_2], \tag{13}$$

where

$$\rho = 2Zr\ , \tag{14}$$

$$n_r = n-|\kappa|\ , \tag{15}$$

$$\gamma = \sqrt{\kappa^2-\alpha^2Z^2}\ , \tag{16}$$

$$N = \sqrt{(n_r+\gamma)^2+\alpha^2Z^2}\ , \tag{17}$$

$$\frac{\epsilon}{c^2} = 1-\sqrt{1-\frac{\alpha^2Z^2}{N^2}}\ , \tag{18}$$

$$\xi = \sqrt{\frac{Z}{2N^2(N-\kappa)}\frac{\Gamma(2\gamma+n_r+1)}{[\Gamma(2\gamma+1)]^2n_r!}}\ , \tag{19}$$

$$F_1 = F(-n_r+1, 2\gamma+1; \frac{\rho}{N})\ , \tag{20}$$

$$F_2 = F(-n_r, 2\gamma+1; \frac{\rho}{N})\ . \tag{21}$$

In contrast to the nonrelativistic case, the analytical form is not given here for relativistic Compton profile because of its extreme complexity. For simplicity, the relativistic Compton profile has been calculated numerically and also listed in Table 1. It is shown that the relativistic effect on the Compton profile is too weak to distinguish them for H atom in Table 1 and Fig. 1.

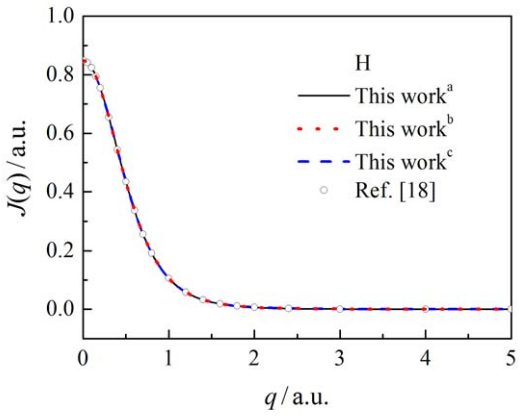

Fig. 1 (color online) Compton profile of $1s$ orbital of H atom.

For Xe^{53+} ion, the present results are apparently different from the values obtained by Eq. (11). It can be seen in Table 1 and Fig. 2 that the relativistic effect decreases the Compton profile in the low momentum region and expands the distribution to the large momentum. In other words, the probability that $1s$ electron in Xe^{53+} ion has the high momentum can reach larger value due to the relativistic effect, so that the relativistic Compton profile must be more diffuse than the nonrelativistic one. From the point of view of radial wavefunction in coordinate space, the relativistic effect can contract the distribution of $1s$ orbital, so its Compton profile can expand into the region of high momentum.

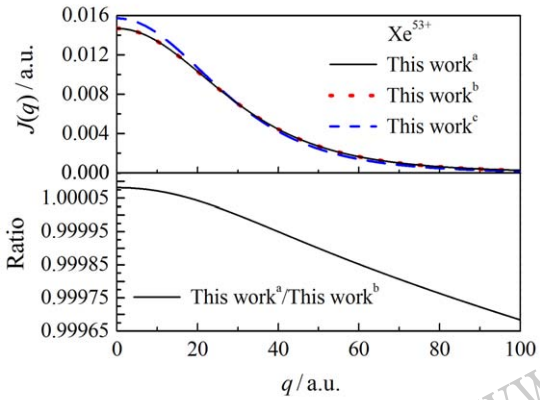

Fig. 2 (color online) Compton profile of $1s$ orbital of Xe^{53+} ion.

In addition, with comparison between the calculation a and b, it is shown that the nuclear volume effects are hardly embodied especially for atomic H in Fig. 1, even though the data give some differences in Table 1. In fact, the differences between the results, respectively from different calculation a and b, could be reduced when the accuracy were improved. For Xe^{53+} ion, there are some slight differences between its Compton profile a and b from Table 1, so the ratio between the calculation a and b are also plotted in Fig. 2. The results show that at the present level of 3 or 4 significant digits, the nuclear volume effects can be neglected for H atom and Xe^{53+} ion.

3.2 Compton profile of the excited states $n\kappa(n=2\sim7)$ in H atom

The Compton profiles of $n\kappa$ $(n=2\sim7)$ orbitals of H atom have been plotted in Figs. $3\sim5$ for better understanding. From these figures, it is found that, no matter what the value of n and κ, there are common property that the Compton profile has some certain number of platforms likewise nodes in spatial radial wavefunction. That is, for given l_j, the number of platforms is $n-l$ and they are in a sudden decreasing manner in turn from small to large momentum. As is well known, the single-electron radial orbitals have the certain number of nodes in coordinate space, therefore their corresponding wavefunction and density in momentum space still have the node structure and then the integration of node structure results in the platforms in their Compton profiles.

Then, it is apparent that at low momentum near q=0 a.u. the Compton profile increases with the increase of the principle quantum number n if given l_j. On the other hand, the Compton profile decreases as increasing n at large momentum of especially *e.g.* $q>0.5$ a.u. when $l\leqslant3$ for H atom shown in Figs. $3\sim4$. In other words, for given l_j, the momentum distribution of the orbital with large n dominates at low momentum near q=0 a.u.. On the contrary, the momentum distribution of the orbital with small n plays an important role in the region of large momentum for the orbital with $l\leqslant3$. For $l>3$, it is shown that the order of the Compton profile is normal for $g_{7/2,9/2}$ and $h_{9/2,11/2}$ orbitals at low momentum as mentioned in the situation for $l\leqslant3$, *i.e.*, $J_{5g_{7/2,9/2}}(0)<J_{6g_{7/2,9/2}}(0)<J_{7g_{7/2,9/2}}(0)$ and $J_{6h_{9/2,11/2}}(0)<J_{7h_{9/2,11/2}}(0)$. But at high momentum it can be seen only that the Compton profile with small n supplies the narrow distribution in Fig. 4.

Generally speaking, one orbital with l can be splitted into two orbitals with $l_{j=l-\frac{1}{2}}$ and $l_{j=l+\frac{1}{2}}$ due to the relatvistic effect except for s orbital. Fig. 5 gives the Compton profiles of $4l_j$ orbitals and the ratios $\frac{J_{nl_{j=l+\frac{1}{2}}}(q)}{J_{nl_{j=l-\frac{1}{2}}}(q)}$ that can be used to describe the extent of relativistic splitting. Apparently, the Compton profiles reduce rapidly for larger orbital quantum number l for given principle quantum number n. At the region of low and high momentum, the orbital quantum number l larger, the Compton profile smaller for given n, e.g. $J_{4s}(0)>J_{4p_{1/2,3/2}}(0)>J_{4d_{3/2,5/2}}(0)>J_{4f_{5/2,7/2}}(0)$ and the Compton profile with smaller l can distribute more diffusely. But for H atom, it is hardly to show their

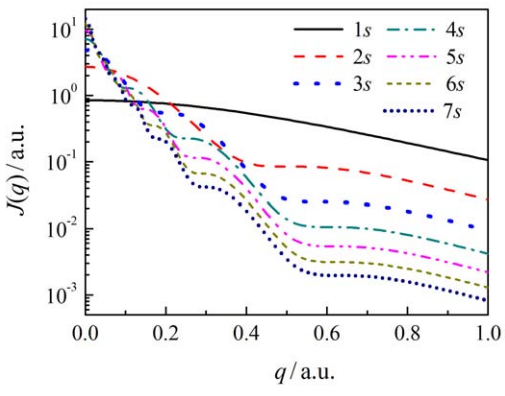

Fig. 3 (color online) Compton profile of ns orbitals of H atom.

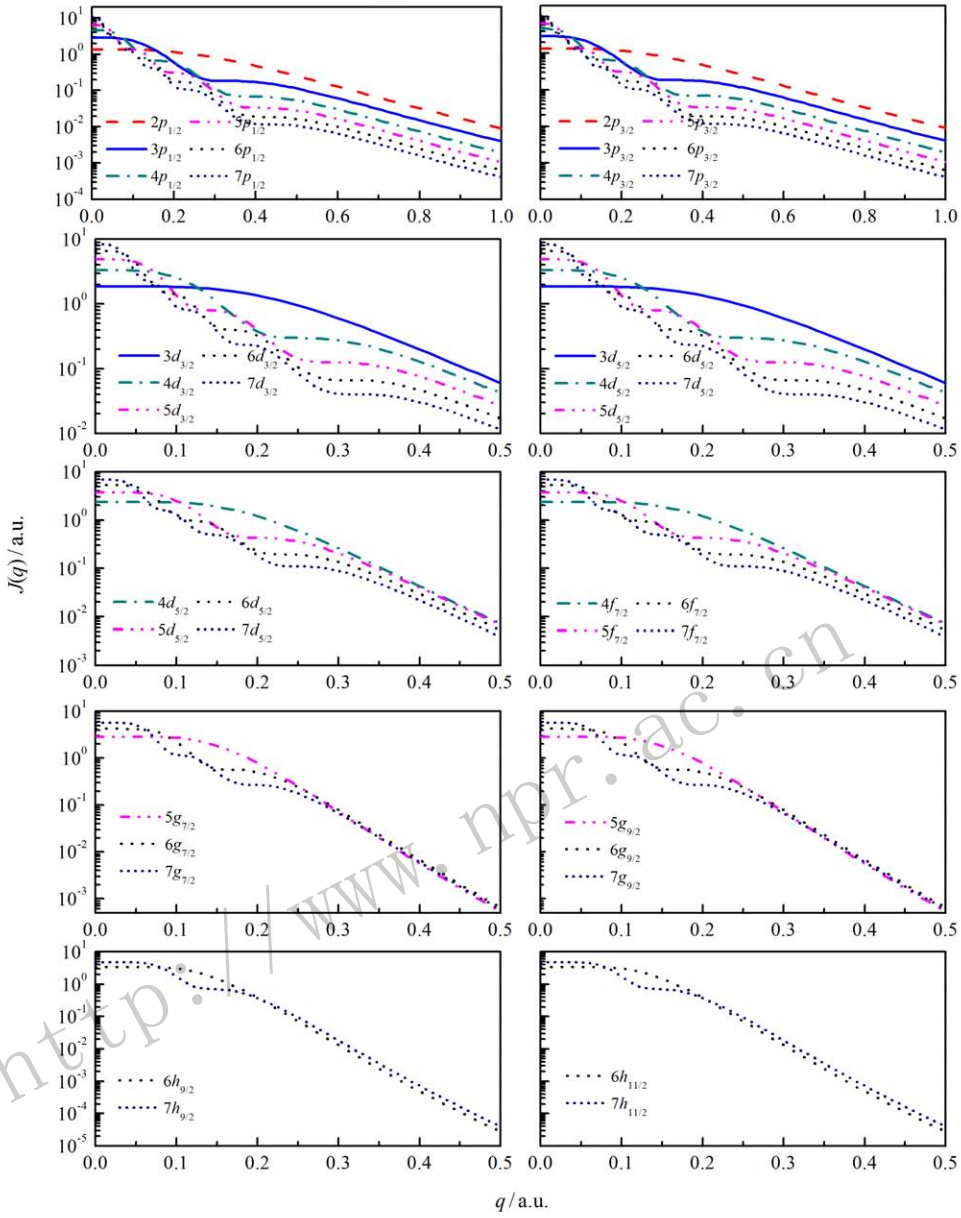

Fig. 4　(color online) Compton profile of $np_{1/2,3/2}$, $nd_{3/2,5/2}$, $nf_{5/2,7/2}$, $ng_{7/2,9/2}$, and $nh_{9/2,11/2}$ orbitals of H atom.

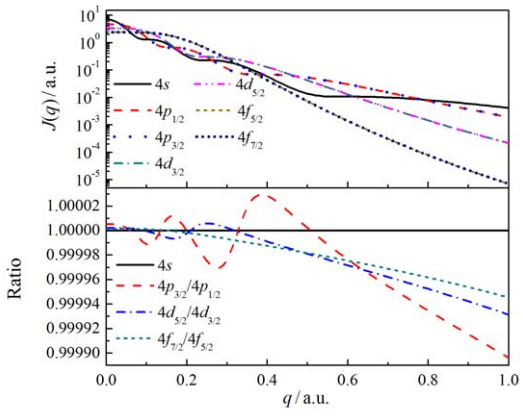

Fig. 5　(color online) Compton profile and relativistic effects of $4l_j$ orbitals of H atom.

differences between two orbitals with $4l_{j=l-\frac{1}{2}}$ and $4l_{j=l+\frac{1}{2}}$. According to the ratio, the relativistic effects result in the different trends. That is, the Compton profiles of the orbitals with $j=l-\frac{1}{2}$ are smaller than that with $j=l+\frac{1}{2}$ at low momentum *i.e.*, $J_{nl_{j=l-\frac{1}{2}}}(0) < J_{nl_{j=l+\frac{1}{2}}}(0)$, while in the region of high momentum q, the Compton profiles of the orbitals with $j=l-\frac{1}{2}$ are larger than that with $j=l+\frac{1}{2}$, *i.e.*, $J_{nl_{j=l-\frac{1}{2}}}(q) > J_{nl_{j=l+\frac{1}{2}}}(q)$. On the other hand, the differences between them gradually disappear as increasing $l>0$, because the ratio approach one with the increase of $l>0$ either near $q=0$ or for large momentum, which indicates the stronger relativistic splitting takes place in those electron state with low orbital quantum

number l for given n.

3.3 Compton profile of the excited states $n\kappa(n=2\sim7)$ in Xe^{53+} ion

Figs. $6\sim8$ show the dependence of the Compton profiles on the momentum q of $n\kappa$ $(n=2\sim7)$ orbitals of Xe^{53+} ion. From these figures, as mentioned in Sec. 3.2, no matter what the value of nl_j, there are certain number of platforms for the orbital with l_j of Xe^{53+} ion. The number of platforms is $n-l$ that is the same as in the situation for H atom. However, the Compton profile is more expanded for Xe^{53+} ion. It is shown that the electron momentum is easier to reach high value comparing with H atom, in fact, as shown in Figs. $1\sim2$.

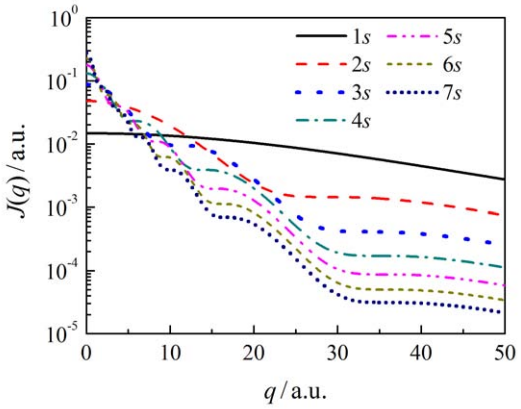

Fig. 6 (color online) Compton profile of ns orbitals of Xe^{53+} ion.

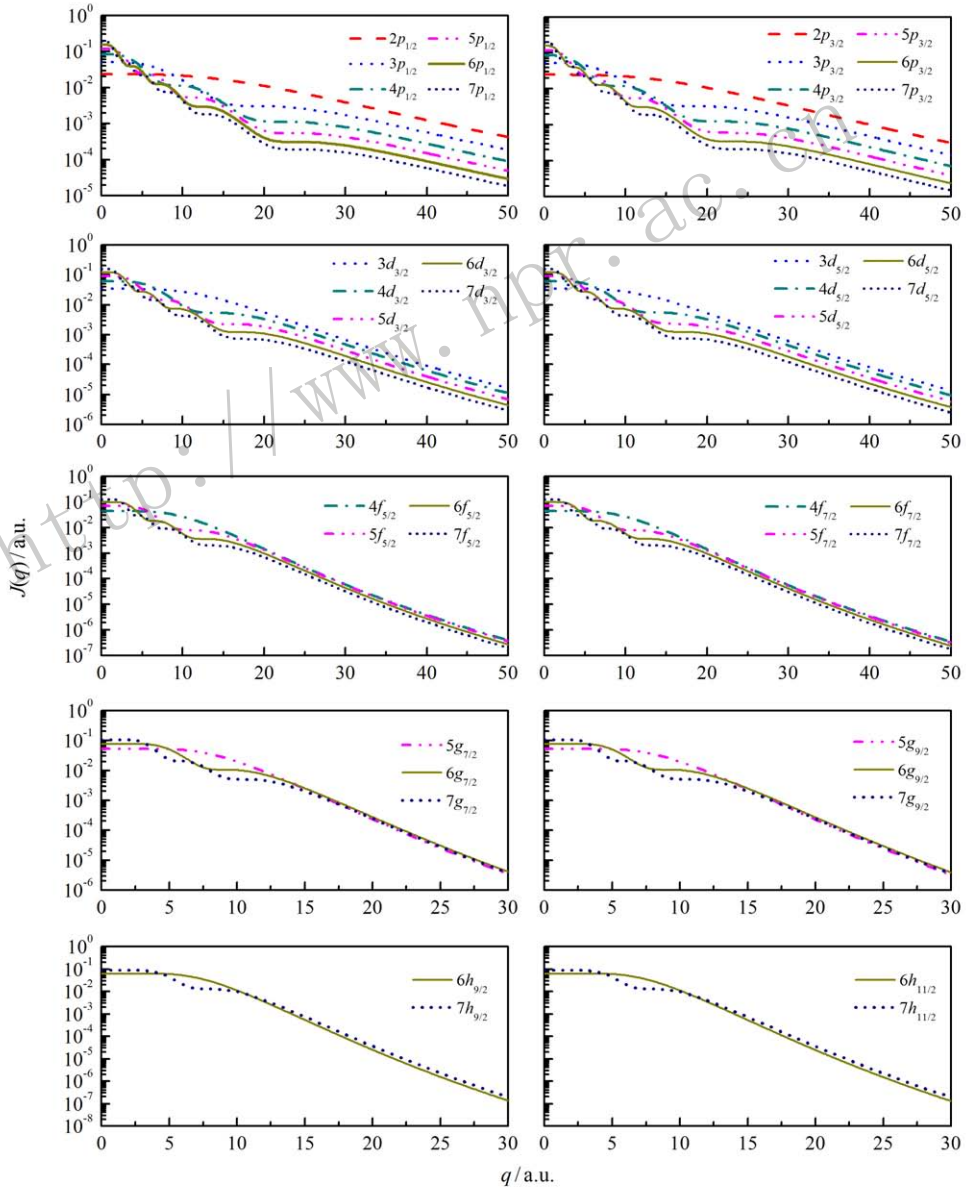

Fig. 7 (color online) Compton profile of $np_{1/2,3/2}$, $nd_{3/2,5/2}$, $nf_{5/2,7/2}$, $ng_{7/2,9/2}$, and $nh_{9/2,11/2}$ orbitals of Xe^{53+} ion.

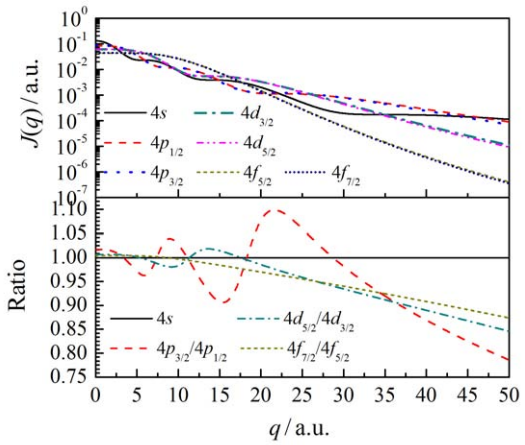

Fig. 8 (color online) Compton profile and relativistic effects of $4l_j$ orbitals of Xe^{53+} ion.

Further, it can also be seen that the Compton profile increases with the increase of the principle quantum number n for the orbitals with given l_j at low momentum near $q=0$ a.u., while the Compton profile goes down with the increase of n at large momentum over $q\sim 30$ a.u. roughly when $l\leqslant 3$ in Figs. 6 ~ 7. The Compton profile of the orbital with large n dominates at low momentum for the orbitals with given l_j, but the Compton profile of the orbital with small n shows the main contribution in the region of large momentum. Likely in H atom, for $l>3$, the order of the Compton profile is normal for $g_{7/2,9/2}$ and $h_{9/2,11/2}$ orbitals at low momentum as mentioned in the situation for $l\leqslant 3$, *i.e.*, $J_{5g_{7/2,9/2}}(0)<J_{6g_{7/2,9/2}}(0)<J_{7g_{7/2,9/2}}(0)$ and $J_{6h_{9/2,11/2}}(0)<J_{7h_{9/2,11/2}}(0)$. However, the Compton profile is smallest for smallest n at high momentum in Fig. 7.

For Xe^{53+} ion, from Fig. 8, the differences are easily shown between the Compton profiles of the orbitals with same l and different j at low momentum. Likely in H atom, the Compton profiles reduce rapidly for larger orbital quantum number l for given principle quantum number n. At the region of low and high momentum, the orbital quantum number l larger, the Compton profile smaller for given n, *e.g.* $J_{4s}(0)>J_{4p_j}(0)>J_{4d_j}(0)>J_{4f_j}(0)$ and the Compton profile with smaller l can distribute more diffusely. However, on the contrary of H atom, the Compton profile of the orbitals with $j=l-\frac{1}{2}$ are smaller than that with $j=l+\frac{1}{2}$ in the region of low momentum, *i.e.*, $J_{nl_{j=l-\frac{1}{2}}}(0)<J_{nl_{j=l+\frac{1}{2}}}(0)$, while the situation is just oppsite in the region of high momentum: $J_{nl_{j=l-\frac{1}{2}}}(q)>J_{nl_{j=l+\frac{1}{2}}}(q)$. The results are similar to those for H atom. Of course, the differences between them with same l and different j still gradually disappear with increasing $l>0$ either near $q=0$ or for high momentum. In addition, Fig. 9 shows the ratios $\frac{J_{nl_{j=l+\frac{1}{2}}}(q)}{J_{nl_{j=l-\frac{1}{2}}}(q)}$ of Xe^{53+} for $n=2-7$ and $l=1-5$. It is clear that the ratio approach one with the increase of n either near $q=0$ or for large momentum, which indicates the stronger relativistic splitting takes place in those orbitals with low principal quantum number n for given l.

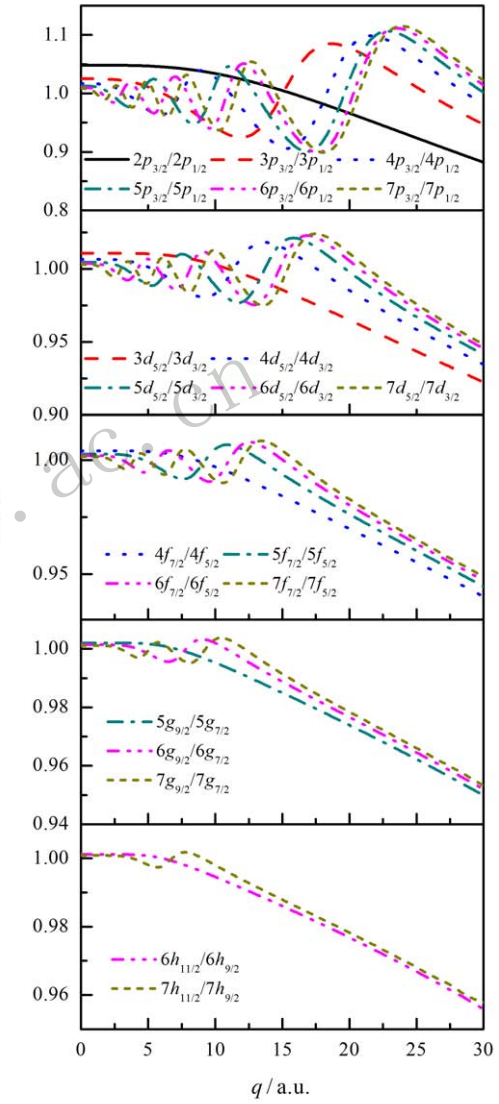

Fig. 9 (color online) Relativistic effects in Compton profile of $nl_j(n=2\sim 7)$ orbitals of Xe^{53+} ion.

4 Conclusions

In this work, the Compton profile of H-like ions has been calculated systematically by using the GRASP code[23] and Fourier transformation. The effects of relativity and nuclear finite size on the Compton profile of the single electron have also been shown in the present results with the help of comparing with the Compton profile obtained from the analytical relativistic and nonrelativistic radial wavefunction in point

Coulomb potential. As is well known, the relativistic effect is apparent for the orbital in atom or ion with large Z. On the contrary of the spatial wavefunction, the effect of relativity can expand the distribution of the Compton profile. On the other hand, the orbital splits are more and more obvious for given $nl(l \neq 0)$ as increasing Z. Of course, likely in spatial wavefunction, the relativistic effect can gradually weaken with the increase of the principal quantum number n and orbital quantum number l. In addition, the nuclear finite size hardly affects the Compton profile for H atom and Xe^{53+} ion.

Furthermore, it is found that the Compton profile of the orbital with quantum number nl_j has certain number of platforms that is $n-l$. The momentum distribution can be more diffused for the ion with larger Z if given the quantum nl_j, which means the orbitals contribute more momentum distribution for atom or ion with small Z near $q = 0$ a.u., while those for ion with larger Z can dominate the distribution in the high momentum.

In fact, the present calculation can also be directly extended to consider the electron correlation effects on Compton profile, if one-electron spatial orbitals were obtained by multiconfiguration self-consistent-field such as multiconfiguration Hartree-Fock and Dirac-Fock methods, where the electron correlation can be included in one-electron radial orbitals to some extent.

References:

[1] CHEN C J. Physics, 1980, **9**: 350. (in Chinese)

[2] BERGSTROM P M, PRATT R H, Radiat Phys Chem, 1997, **50**: 3.

[3] PRATT R H, LAJOHN L A, FLORESCU V, SURIĆ T, CHATTERJEE B K, ROY S C. Radiat Phys Chem, 2010, **79**: 124.

[4] MANNINEN S. J Phys Chem Solids, 2000, **61**: 335.

[5] EICHLER J, STÖHLKER Th. Phys Rep, 2007, **439**: 1.

[6] CURRAT R, DECICCO P D, WEISS R J. Phys Rev B, 1971, **4**: 4256.

[7] PANT M M, TALMAN J D. Phys Rev A, 1978, **17**: 1819.

[8] TONG B Y, LAM L. Phys Rev A, 1978, **18**: 552.

[9] MUKHOPADHYAYA S, RAY S N, TALUKDAR B. J Chem Phys, 1982, **76**: 2484.

[10] PARR R G, RUPNIK K, GHOSH S K. Phys Rev Lett, 1986, **56**: 1555.

[11] HOLM P. Phys Rev A, 1988, **37**: 3706.

[12] KARIM KR. J Quant Spectrosc Radiat Transfer, 2003, **77**: 13.

[13] KARIM KR. J Quant Spectrosc Radiat Transfer, 2006, **98**: 68.

[14] LI B, LI G Q, DENG J K, Gao H. Chin J Compt Phys, 2004, **21**: 117. (in Chinese)

[15] HARBOLA M K, ZOPE R R, KSHIRSAGAR A, PATHAK R K. J Chem Phys, 2005, **122**: 2041101.

[16] JAISWAL P, SHUKLA A. Phys Rev A, 2007, **75**: 022504.

[17] MOU Z D, WEI Q Y, DING K, YE S W. J Atom Mole Phys, 2010, **27**: 19. (in Chinese)

[18] BIGGS F, MENDELSOHN L B, MANN J B. Atomic data and nuclear data tables, 1975, **16**: 201.

[19] THAKKAR A J, WONFOR A L, PEDERSEN W A. J Chem Phys, 1987, **87**: 1212.

[20] KOGA T, MATSUYAMA H. Phys Rev A, 1992, **45**: 5266.

[21] KOGA T, MATSUYAMA H, INOMATA H, ROMERA E, DEHESA J S, THAKKAR A J. J Chem Phys, 1998, **109**: 1601.

[22] DYALL K G, GRANT I P, JOHNSON C T, PARPIA F A, PLUMMER E P. Comput Phys Commun, 1989, **55**: 425.

[23] PARPIA F A, FISCHER C F, GRANT I P. Comput Phys Commun, 1996, **94**: 249.

[24] GRANT I P. Relativistic Quantum Theory of Atoms and Molecules[M]. New York: Springer, 2007.

[25] SURZHYKOV A, KOVAL P, FRITZSCHE S. Comput Phys Comm, 2005, **165**: 139.

[26] BURKE V M, GRANT I P, Proc Phys Soc, 1967, **90**: 297.

类氢离子的相对论康普顿轮廓

万建杰[1)]

（西北师范大学物理与电子工程学院，兰州 730070）

摘要： 基于中心场近似得到Dirac径向轨道，并使用恰当的Fourier变换系统计算了类氢离子电子动量分布和康普顿轮廓。以H原子和Xe^{53+}离子为例，探讨了相对论效应和原子核的有限体积效应对单电子康普顿轮廓的影响。同时，详细研究了单电子康普顿轮廓对主量子数n、轨道量子数l、单电子总角动量量子数j和核电荷数Z的依赖关系。结果表明，相对论效应可以扩展康普顿轮廓的分布,并且使给定nl的轨道随着Z的增加分裂得越来越明显。然而，相对论效应也会随着主量子数n和轨道量子数l的增加而减弱。同时，对于nl_j轨道，其康普顿轮廓还具有$n-l$个平台的结构。另外，原子核的有限体积几乎不会影响H原子和Xe^{53+}离子的康普顿轮廓。

关键词： 康普顿轮廓；相对论效应；电子动量分布；类氢离子

收稿日期： 2016-06-08；　**修改日期：** 2016-09-18

基金项目： 国家自然科学基金青年科学基金项目(11204243)；甘肃省自然科学基金青年科技计划(1506RJYA131)；西北师范大学物理与电子工程学院物理学科科研创新团队项目资助

1) E-mail: wanjj@nwnu.edu.cn。